Earth Surface Processes and Landforms
Earth Surf. Process. Landforms **32**, 544–560 (2007)
Published online 11 September 2006 in Wiley InterScience
(www.interscience.wiley.com) **DOI:** 10.1002/esp.1407

Quantifying hillslope erosion rates and processes for a coastal California landscape over varying timescales

Colin R. O'Farrell, Arjun M. Heimsath* and James M. Kaste
Department of Earth Sciences, Dartmouth College, 6105 Fairchild Hall, Hanover, NH 03755, USA

**Correspondence to: A. M. Heimsath, Department of Earth Sciences, Dartmouth College, 6105 Fairchild Hall, Hanover, NH 03755, USA. E-mail: Arjun.Heimsath@Dartmouth.edu*

Abstract

The Earth's surface erodes by processes that occur over different spatial and temporal scales. Both continuous, low-magnitude processes as well as infrequent, high-magnitude events drive erosion of hilly soil-mantled landscapes. To determine the potential variability of erosion rates we applied three independent, field-based methods to a well-studied catchment in the Marin Headlands of northern California. We present short-term, basin-wide erosion rates determined by measuring pond sediment volume (40 years) and measured activities of the fallout nuclides ^{137}Cs and ^{210}Pb (40–50 years) for comparison with long-term (>10 ka) rates previously determined from *in situ*-produced cosmogenic ^{10}Be and ^{26}Al analyses. In addition to determining basin-averaged rates, ^{137}Cs and ^{210}Pb enable us to calculate point-specific erosion rates and use these rates to infer dominant erosion processes across the landscape. When examined in the context of established geomorphic transport laws, the correlations between point rates of soil loss from ^{137}Cs and ^{210}Pb inventories and landscape morphometry (i.e. topographic curvature and upslope drainage area) demonstrate that slope-driven processes dominate on convex areas while overland flow processes dominate in concave hollows and channels. We show a good agreement in erosion rates determined by three independent methods: equivalent denudation rates of 143 ± 41 m Ma^{-1} from pond sediment volume, 136 ± 36 m Ma^{-1} from the combination of ^{137}Cs and ^{210}Pb, and 102 ± 25 m Ma^{-1} from ^{10}Be and ^{26}Al. Such agreement suggests that erosion of this landscape is not dominated by extreme events; rather, the rates and processes observed today are indicative of those operating for at least the past 10 000 years.

Received 8 September 2005;
Revised 2 May 2006;
Accepted 5 June 2006

Keywords: ^{137}Cs; ^{210}Pb; cosmogenic nuclides; geomorphology; landscape evolution

Introduction

Quantifying erosion rates and processes is central to our understanding of how landscapes evolve under climatic, tectonic, and anthropogenic forcing. Recent work (e.g. Kirchner *et al*., 2001; Campbell and Church, 2003; Hewawasam *et al*., 2003; Gellis *et al*., 2004; Lavè and Burbank, 2004) quantifies how landscape-scale erosion rates can vary with dominant erosional process, and suggests that measurements capturing different timescales might reflect the dominance of different processes. Any temporal variability has consequences for attempts to characterize landscape erosion rates based on processes currently dominant. For example, episodic, high-magnitude events (landslides, floods) may be a dominant source of sediment and may not be captured by suspended-sediment studies capturing annual to decadal timescales (Dietrich and Dunne, 1978). Using independent tools to decipher erosion rates operating over both short- and long-term timescales is therefore ideal. Understanding the temporal variability in hillslope sediment loss also has implications for land management issues, such as agriculture, stream health and civil planning (e.g. Huang and O'Connell, 2000; Bonnet and Crave, 2003; Flint *et al*., 2003; Litvin *et al*., 2003). In this study we examine a

well-studied, soil-mantled upland landscape where long-term erosion rates were previously quantified using *in situ*-produced cosmogenic nuclides (Heimsath *et al*., 1997, 1999). We focus on quantifying short-term rates using two independent methods and then compare the results with the long-term rates. Specifically, we use short-lived, fallout-derived nuclides as well as measurements of sediment stored in a stock pond.

Anthropogenic ^{137}Cs ($t_{1/2} = 30{\cdot}1$ years) and naturally occurring excess ^{210}Pb (half-life, $t_{1/2} = 22{\cdot}3$ years; 'excess' is the amount of ^{210}Pb above the level supported by soil ^{222}Rn) have gained wide use in recent years as tracers of soil movement (e.g. Wallbrink and Murray, 1993, 1996; Porto *et al*., 2001; Walling and He, 1999; Matisoff *et al*., 2002). Given their half-lives and unique atmospheric source term, these fallout nuclides are useful for calculating and tracing soil loss over decadal timescales. The methodology relies on the assumption that once ^{137}Cs and ^{210}Pb reach the soil, they are strongly adsorbed and can only be redistributed with soil movement. Erosion and deposition rates are determined by comparing the radionuclide inventories and profiles (with depth in the soil) to the inventory at a stable, non-eroding reference site (Walling and He, 1999; Walling *et al*., 2003).

Short-lived radionuclides are a powerful tool that enable the calculation of point erosion rates, as well as the spatial variability of erosion rates across a landscape with only a single field visit (Walling and He, 1999; Walling *et al*., 1999). Point-specific measurements can also be used with land surface morphometry to differentiate dominant erosional processes. For example, if point erosion rates correlate with upslope contributing area, then overland flow may be a dominant process (Kaste *et al*., 2006). Conversely, correlation of erosion with topographic curvature would support a linear diffusion-like transport processes (e.g. Carson and Kirkby, 1972; Dietrich *et al*., 2003). With sufficient sampling density or morphometric correlation point-specific rates may then be integrated using an appropriate digital elevation model (DEM) to determine basin-wide rates (Walling *et al*., 2002).

Anthropogenic ponds and reservoirs of known age have been widely used to determine basin-wide erosion rates over timescales which vary from several months to 200 years (e.g. Huang and O'Connell, 2000), depending on the lifespan of the water body (see review in Verstraeten and Poesen, 2000). Sediment traps have also been used in concert with fallout nuclides to validate the radionuclide calibration equations for quantitatively determining soil loss from inventory depletion (e.g. Zhang *et al*., 1997; Porto *et al*., 2001). Here, we use volumetric estimates of sediment trapped in a stock pond of known age at the outlet of our study catchment to calculate a basin-wide erosion rate valid over the lifespan of the pond. We compare this basin-averaged, short-term rate with an array of point-specific measurements of short-lived fallout nuclides from soil pits. We conclude by comparing our short-term rates with the long-term (>10 ka), basin-wide erosion rates determined using cosmogenic nuclide (^{10}Be and ^{26}Al) concentrations reported in Heimsath *et al*. (1997, 1999).

Study Area

The Haypress basin ($0{\cdot}33$ km^2) is a small tributary of Tennessee Valley in the Marin Headlands of northern California (Figure 1). The study catchment and surrounding landscape are extensively studied (e.g. Reneau *et al*., 1984, 1990; Montgomery and Dietrich, 1988, 1989, 1994; Dietrich *et al*., 1992, 1993, 1995; Heimsath *et al*., 1997, 1999), and are underlain by deformed greywacke, chert, and greenstone of the Franciscan assemblage (Wahrhaftig, 1984). The climate is Mediterranean, with annual precipitation of *c*. 760 mm (Rantz, 1968), primarily occurring from November to March. During winter rainstorms, saturation overland flow can develop in the unchannelled, colluvium-filled hollows (Wilson and Dietrich, 1987; Dietrich *et al*., 1993; Montgomery and Dietrich, 1994; Prosser *et al*., 1995).

Elevations range from 100 m to 314 m, with gentle slopes on ridge tops, steepening to nearly 40° just above the broad valley bottom. Coastal grasses cover most ridge tops and convex noses, while thick stands of poison oak (*Rhus diversiloba*) and coyote bush (*Baccharis pilularis*) occupy the hollows. Woody scrub has been progressively covering more of the landscape since 1983 when the National Park Service took ownership of the land and ended *c*. 130 years of cattle grazing (United States Geological Survey (USGS) aerial photos; Stewart, personal communication). Soil thickness varies considerably, from *c*. 15 cm along sharply divergent ridge crests to 1–2 m in the unchannelled hollows (Heimsath *et al*., 1997, 1999). Across the grassy slopes, pocket gopher (*Thomomys bottae*) burrows and tailings piles are obvious and widespread. Soil transport by gophers is thought to be the primary mechanism for diffusion-like downslope soil transport (Black and Montgomery, 1991). The catchment of interest is identified as sub-basin 2 in Heimsath *et al*. (1999) and is shown here in Figure 1. A former landowner impounded Haypress Creek behind an earthen dam some time between 1953 and 1968 to create Haypress Pond, intended for use as a cattle-watering station (USGS aerial photos; Stewart, personal communication). Haypress pond thus served as a natural sediment trap, retaining sediment delivered from the hillslopes, until the US Park Service removed the dam in 2003 as part of a stream restoration project. Pond sediment parameters are given in Table I.

DOI: 10.1002/esp

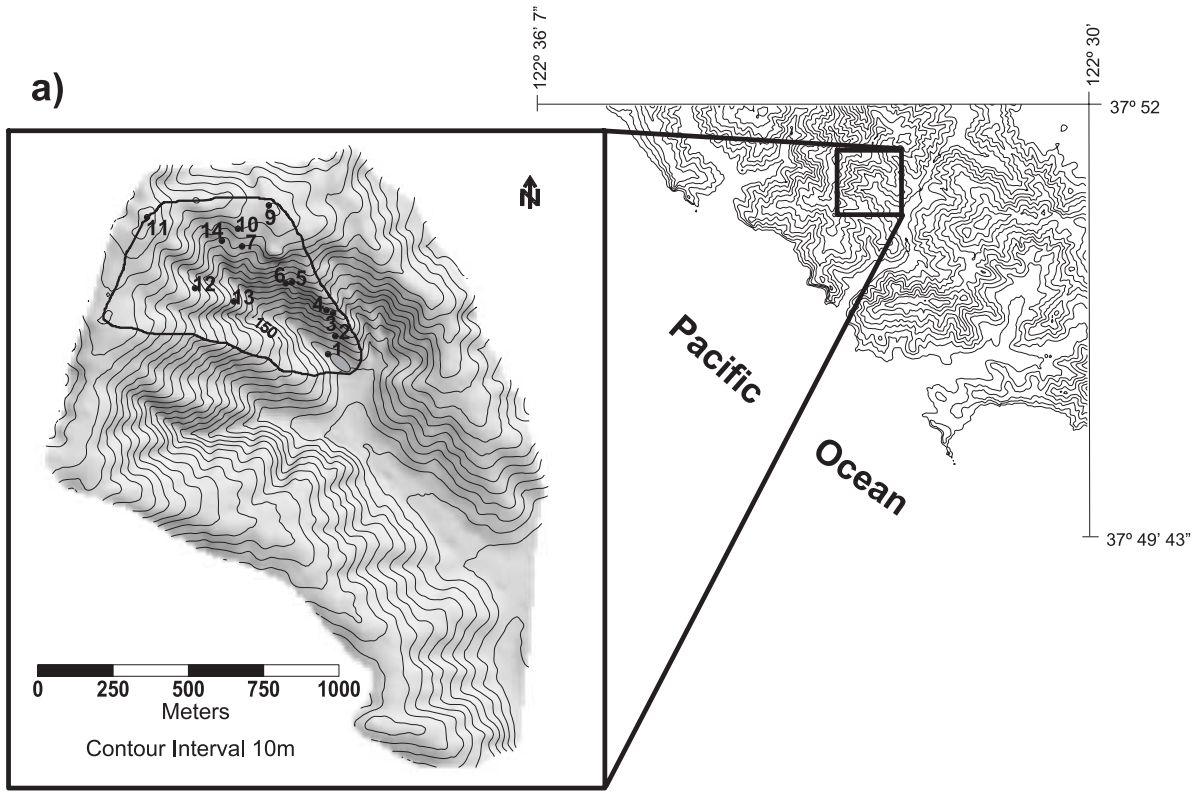

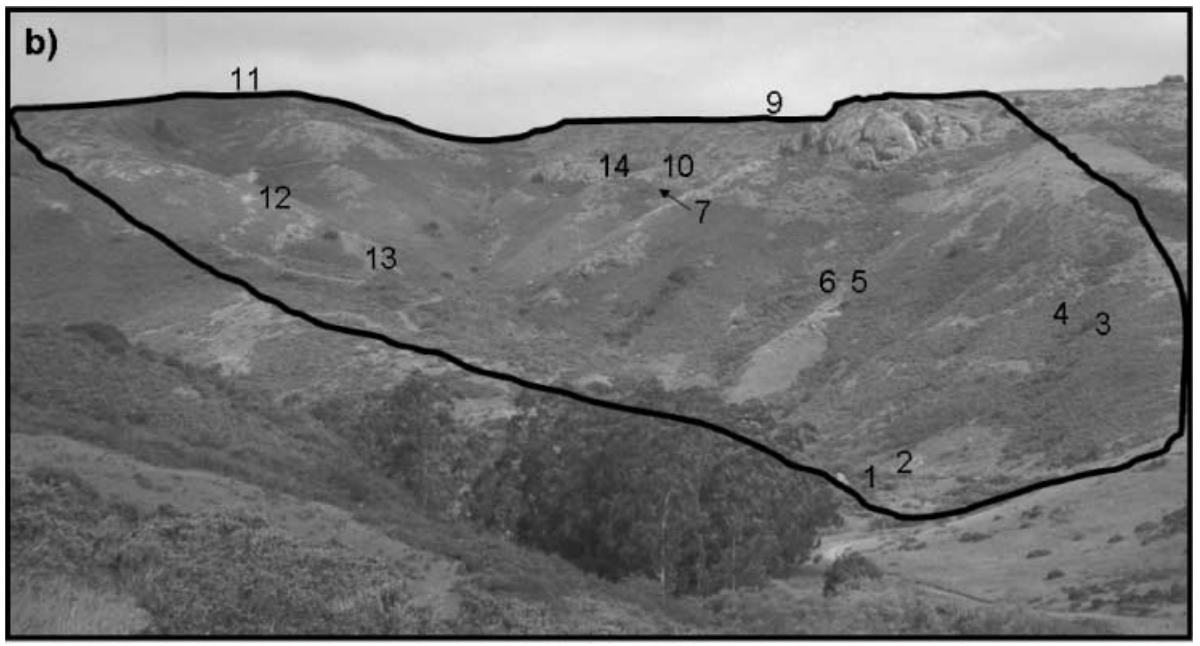

Figure 1. (a) Site location for Tennessee Valley, Marin County, California, USA. Regional topography is shown from part of the Point Bonita, CA USGS 7·5 min quadrangle with 30 m contours. Inset contour map is based on high-resolution digital data with 10 m contours and shows the study catchment outlined with black line, radionuclide sampling pits (numbered by pit), and Haypress Pond as the white patch at base of the catchment. (b) Photograph of the study area, with the Haypress catchment outlined in black and rough locations of radionuclide sampling pits indicated with pit numbers. Haypress Pond is located immediately downhill of pit 1.

DOI: 10.1002/esp

Table I. Pond sediment parameters

Parameter	Value
Surveyed pond sediment volume (m^3)	655 ± 130
Trap efficiency (%)	17
Bedrock density (kg m^{-3})	2200
Dry pond sediment density (kg m^{-3})	700
Pond age (years)	42 ± 8
Catchment area (ha)	33

Conceptual Framework and Methods

Pond sediment volume

Upon entering a holding pond, energetic stream waters carrying sediment slow down and deposit their suspended sediment load. Volume determination of pond sediment deposits is extensively used to quantify basin-wide sediment yield from small catchments (e.g. McManus and Duck, 1985; Van den Wall Bake, 1986; Neil and Mazari, 1993; Verstraeten and Poesen, 2002). The volume of sediment retained in the pond does not necessarily represent 100 per cent of the sediment delivered to any given pond. Often, a pond can trap only some fraction of the sediment delivered to it, where the trap efficiency (*TE*) of the pond depends on annual stream discharge, catchment drainage area, and the pond capacity (Vertsraeten and Poesen, 2000). We determined the *TE* for Haypress Pond using Heinemann's (1981) curve for small agricultural ponds, which predicts *TE* as a function of the annual inflow:pond capacity ratio. The total amount of sediment delivered to the pond from the catchment is simply the measured volume of pond sediment, V (in m^3), divided by *TE*. Using the dry bulk density of the pond sediments, ρ_{ds} (in kg m^{-3}), the total sediment mass, M (in kg), eroded from catchment is (Verstraeten and Poesen, 2002):

$$M = \rho_{ds}\left(\frac{V}{TE}\right) \tag{1}$$

Using an average bedrock bulk density (ρ_{br}) for the parent material contributing sediment to the pond enables the calculation of a basin-wide bedrock-lowering rate, E (in m a^{-1}), based on the mass of the pond sediment:

$$E = \frac{M}{\rho_{br}}\frac{1}{A^{*}t} \tag{2}$$

where A is the contributing area (in m^2) and t is the pond age (in years). We collaborated with the US Park Service stream restoration project to gain access to the pond prior to and following its draining. We cored the pond sediments to determine sediment thicknesses using a small rowboat and a direct-push corer (Figure 2). Following draining of the pond and removal of the dam, we determined sediment depths at the pond edges and verified some of our push-core measurements.

Fallout nuclides and transport processes

Using fallout ^{137}Cs and ^{210}Pb as tools for quantifying erosion relies on our comparison between nuclide profiles measured in eroding soil with nuclide profiles measured in soil at reference areas where mass loss/gains can be assumed minimal on short (<100 years) timescales. Nuclide depletion (or enrichment) can be converted to quantitative point estimates of soil loss (or gain) using calibration models (e.g. Walling and He, 1999; Fornes *et al*., 2005), which, given sufficient sampling density, can be integrated to yield a catchment average soil loss rate (cf. Porto *et al*., 2001). In cases where sampling density is too sparse to permit direct interpolation of nuclide-derived erosion rates, correlation of nuclide inventories with landscape parameters thought to be driving erosion may be used to extrapolate the point measurements across a catchment (e.g. Walling *et al*., 2002).

We collected soil samples from 13 pits excavated across the full range of topography from the Haypress catchment (Figure 1). The soil column at each pit was sampled in 2·5 to 5 cm increments from the ground surface to 50 cm depth, or the bedrock–soil boundary, whichever came first. Seven of the sampled pits were analysed in two sections:

DOI: 10.1002/esp

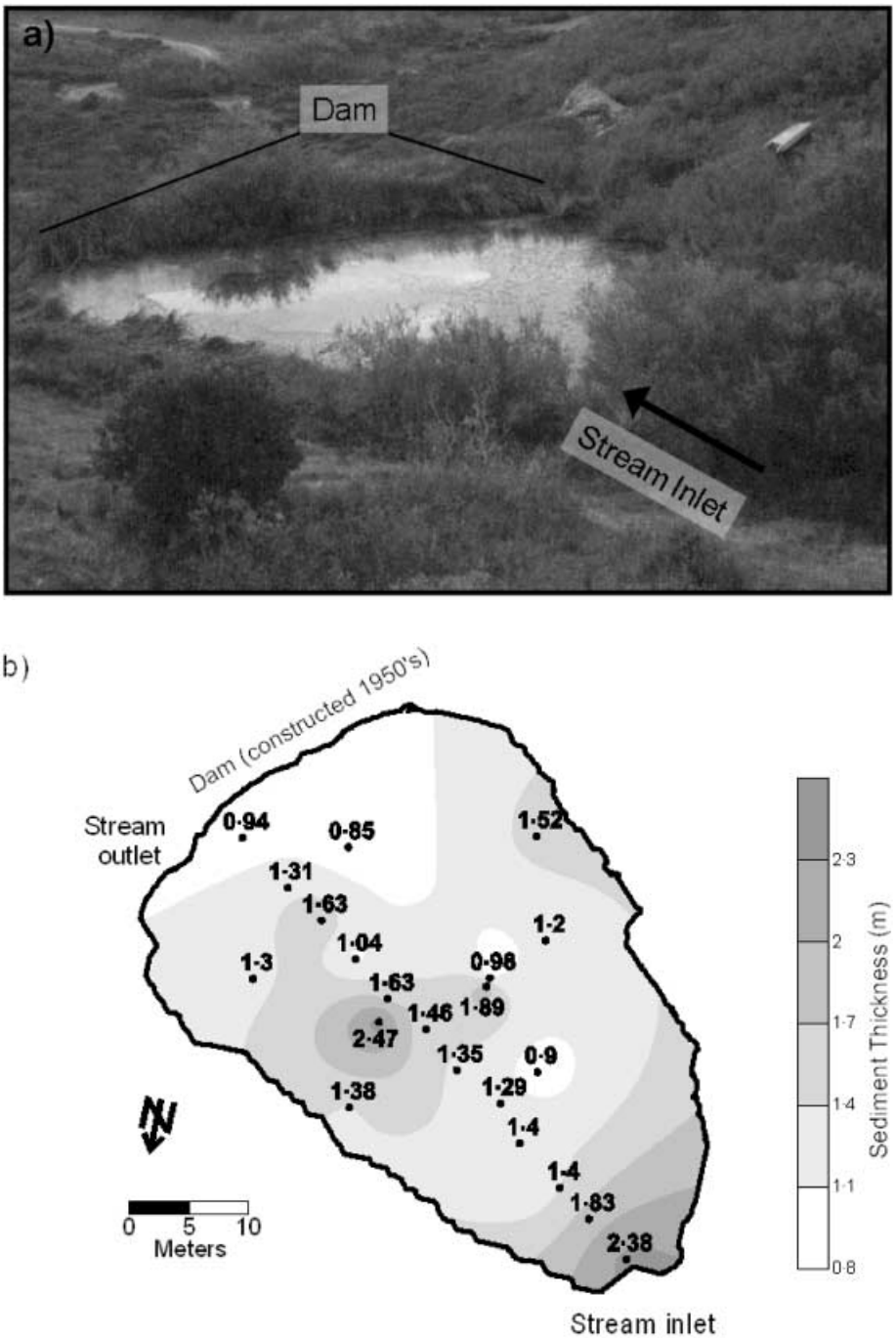

Figure 2. (a) Photograph of stock watering pond constructed in the mid-1950s at the base of the Haypress catchment, taken in November 2002. Photo faces southeast and includes earthen dam that impounds pond, dirt access road from the main Tennessee Valley, as well as surrounding hillslope – pit 2 was dug just upslope of the foreground. The inflatable rowboat (c. 3 m long) used for sampling is on the bank at the upper right of the photo. (b) Map of Haypress Pond showing sediment depth sampling locations and depths (m) from push-core survey. Sediment thickness contours were interpolated from surveyed depths using Golden Software Surfer 8® software. Overall sediment volume was determined using bathymetric surface area and measured sediment thicknesses.

DOI: 10.1002/esp

from 0 to 2·5 cm and from 2·5 to 30 cm, bulked, while the remaining six pits were analysed at 2·5 to 5 cm intervals, allowing us to examine the shape of the radionuclide depth-profile. Pits 9 and 11 were sampled on the nearly flat crest of the catchment, locations where field evidence and previous cosmogenic nuclides analyses suggested the lowest erosion rates for the catchment (Heimsath *et al*., 1997, 1999), and were used as reference sites. All samples were sieved to less than 2 mm and packed in plastic containers for determination of ^{210}Pb, ^{226}Ra and ^{137}Cs via gamma-ray spectrometry at Dartmouth College.

We use inventories of $^{210}Pb_{ex}$ and ^{137}Cs measured in soil profiles across the Haypress Basin to estimate erosion on different parts of the landscape. Models that relate radionuclide inventories to soil erosion rates take into account (a) the temporal distribution of atmospheric nuclide inputs, (b) the vertical migration of nuclides through soil, and (c) the preferential removal of small particles (and thus high surface area) during erosion. Since ^{137}Cs was introduced to soils in a 'pulse' during the 1950s and 1960s, and ^{210}Pb is delivered to soils in more of a steady state, each nuclide requires a unique model when relating inventories to soil loss. We adopt the model of Walling *et al*. (2003) for describing $^{210}Pb_{ex}$ removal from soils:

$$\int_0^t PRC_u\,(t')e^{-\lambda(t-t')}dt' = A(t) \tag{3}$$

where C_u is the concentration of $^{210}Pb_{ex}$ (Bq kg^{-1}) in the top of the soil, A is the amount of $^{210}Pb_{ex}$ (Bq m^{-2}) removed from the soil by erosion annually, R is the erosion rate (kg m^{-2} a^{-1}), λ is the decay rate of ^{210}Pb (0·0311 a^{-1}) and P is the particle size correction factor that we determined by measuring the mean surface diameter of soils sampled on hillslopes and sediments from the pond, which presumably represents mobilized soil (He and Walling, 1996). This model assumes a relatively steady annual input of $^{210}Pb_{ex}$, which is calculated by using reference soil pits, and a steady erosion rate over the past c. 100 years. The advection (V, in mm a^{-1}) and diffusion (D, cm^2 a^{-1}) coefficients were calculated by fitting a traditional advection–dispersion model to the radionuclide depth profiles.

The model that relates measured ^{137}Cs inventories to erosion is similar in concept to the one described above, and incorporates similar parameters. However, steady-state atmospheric input cannot be assumed for weapons fallout. As we did not have ^{137}Cs input data for our site, we used a power-law approximation of the Diffusion and Migration Model for undisturbed soils presented by Walling and He (1999) to calculate soil loss from the measured ^{137}Cs inventory depletion relative to the stable reference pits. The power law approximation is:

$$E = (k_1 D^{e_1} + k_2 V^{e_2} + k_3 H^{e_3} + k_4 P^{e_4})R \tag{4}$$

where E is soil loss rate, R is percentage radionuclide loss relative to a reference inventory, $k_1 - k_4$ and $e_1 - e_4$ are coefficients used to approximate the erosion-nuclide depletion curves given by Walling and He (1999). We measured D, V and P (described above), and use values of H (which approximates the initial penetration of ^{137}Cs during rainfall) observed by Walling and He (1999). We focused our power-law approximation of the erosion–depletion curves around a mean nuclide depletion of 32 per cent, which was most typical for the Haypress catchment, and values of the coefficients and exponents were calculated by optimizing the fit to match the shapes of the curves given in figure 4 of Walling and He (1999). For example, the resulting local slope of our approximation in the region of 32 per cent radionuclide depletion is 0·07. Since pit 1 has 37 per cent ^{137}Cs depletion (Table II), our power-law approximation yields a soil loss rate of 2·6 t ha^{-1} a^{-1}. We calculated short-term soil loss rates for each of our pits using Equations 3 and 4, and converted from units of tonnes per hectare per year (t ha^{-1} a^{-1}) to metres per million years (m Ma^{-1}) to determine equivalent bedrock-lowering rates assuming local steady state using an average saprolite bulk density for the region of 2200 kg m^{-3} (Heimsath *et al*., 1997).

The relatively sparse sampling density of our sample locations rates precluded a simple averaging to determine a basin-wide rate. Instead, similar to Walling *et al*. (2002), we correlated radionuclide inventories with topographic parameters using a high-resolution DEM of the basin (Heimsath *et al*., 1999) and used the topographic correlations to extrapolate an inventory-based erosion rate for the catchment. Specific landscape parameters chosen as proxies for the dominant erosional process depend on the applicable geomorphic transport law (GTL; cf. Dietrich *et al*., 2003) and enable a partitioning the landscape on the basis of these processes (e.g. Carson and Kirkby, 1972).

Specifically, the broad, relatively low-gradient convex noses surrounding the Haypress basin are indicative of a landscape where downslope sediment transport flux is likely to be controlled by linearly slope-dependent processes such that the flux, Q_d (l^3 l^{-1} t^{-1}), can be written in one dimension, for example, as:

$$Q_d = -K_d \frac{dz}{dx} \tag{5}$$

DOI: 10.1002/esp

Table II. Landscape morphometric parameters and inventories for fallout radionuclide sampling sites

Pit no.	Drainage area (m^2)	Slope (deg)	Curvature (1/m)	^{137}Cs Inventory ($Bq\ m^{-2}$)	^{137}Cs depletion (%)	^{210}Pb Inventory ($Bq\ m^{-2}$)	^{210}Pb depletion (%)
1	330000	3	0·030	676	37	1110	35
2	407	23	0·009	633	41	1415	17
3	4600	19	0·008	477	56	368	78
4	223	38	−0·024	640	41	497	71
5	73542	29	0·051	579	46	883	48
6	170	36	−0·014	1180	−9	1112	35
7	98822	29	0·002	556	48	1178	31
9*	67	6	−0·001	1057	2	1508	12
10	170	19	−0·016	1173	−9	1305	24
11*	0·001	3	−0·026	1102	−2	1904	−11
12	576	20	−0·013	1164	−8	1248	27
13	9192	31	−0·014	591	45	762	55
14	400	21	0·020	373	65	609	64

Drainage areas manually delineated using a 10 m contour map.
Slope from field inclinometer measurements.
Curvature calculated from digital elevation model (10 m resolution).
* Stable reference sites.

The constant of proportionality, K_d, is informally known as the diffusion coefficient ($l^2\ t^{-1}$), z is land surface elevation and x is downslope distance. The principal agents of soil transport in such landscapes are bioturbation by gophers and wetting and drying of soil, while aeolian processes are negligible due, in part, to the extensive vegetative cover (Black and Montgomery, 1991; Gabet, 2000; Roering *et al*., 2002). As soil particles are transported downslope they are also mixed vertically into the soil column (Dietrich *et al*., 2003; Heimsath *et al*., 2002). Burrowing gophers accentuate this effect with their tailings piles, and contribute to the well-mixed character of soils observed across the convex noses.

The divergence of sediment transport flux is equivalent to the erosion, or landscape-lowering rate, dz/dt (e.g. Culling, 1960), such that differentiating Equation 5 leads to:

$$\frac{dz}{dt} = -K_d \nabla^2 z = E \tag{6}$$

This widely used equation shows that in areas where linearly slope-dependent processes are dominant, land surface lowering (E) is proportional to topographic curvature. Heimsath *et al*. (1997, 1999) confirm that strongly convex-up (i.e. large values of negative curvature) areas of the study site yield the highest soil production rates, which equal erosion rates assuming local steady-state soil thickness, and that the rates decline with decreasing convexity. If this conceptual framework is applicable and used with the fallout nuclide technique for quantifying soil loss, then nuclide depletion should decrease with decreasing curvature for the convex-up regions of the landscape.

Conversely, concave-up, or convergent, areas such as channels, hollows and swales are generally indicative of advective erosional processes controlled by the discharge of water, where upslope contributing area, A, is shown to be a proxy for discharge (see review in Whipple and Tucker, 1999). Equation 5 can be modified such that:

$$Q_w = -K_w A^m S^n \tag{7}$$

where Q_w is the sediment flux due to advective processes, S is local slope (dz/dx), and K_w, m and n are all field-determined parameters. K_w combines the effects of lithology, climate, vegetation and other factors affecting sediment transport (e.g. Whipple and Tucker, 1999). Kirkby (1969) suggested that the values of m and n might reflect the dominant erosional process. Larger values of m will weight drainage area more heavily and suggest the importance of water-driven sediment flux. Conversely, larger values of n would indicate more strongly slope-dependent processes. Correlation between point estimates of soil loss from fallout radionuclide depletion and Q_w would support Equation 7 as a model for sediment transport. Overland flow processes would result in pronounced soil loss at the top of the soil column, corresponding to the maximum downslope shear stress. In this case, deeper soils would not be affected until the surface soils have been mobilized. This preferential removal of the top of the soil column by advective processes

DOI: 10.1002/esp

differs from the vertical mixing and transport due to diffusion-like processes. As the majority of fallout radionuclide inventory is located in the upper several centimetres of the soil column (He and Walling, 1997), overland flow processes should therefore result in greater inventory depletion than bioturbation processes. Similarly, nuclide inventory depletion should increase with increasing contributing area if advective processes are dominant.

Cosmogenic nuclides

Finally, to evaluate the short-term rates determined with the above methods, we draw on long-term rates from cosmogenically produced nuclides. Long-term erosion rates for the Haypress basin valid over >10 000-year timescales have been determined by Heimsath *et al.* (1997) using the abundances of *in situ*-produced ^{10}Be and ^{26}Al in quartz grains (see reviews of the methodology in Lal, 1991; Nishiizumi *et al.*, 1993; Bierman, 1994; Cerling and Craig, 1994). ^{10}Be and ^{26}Al are produced at a known rate within quartz grains by incident cosmic rays, as a function of latitude, elevation and topographic shielding (Lal, 1991; Nishiizumi *et al.*, 1989). Additional corrections must be made for slope and soil thickness of the sample site (Nishiizumi *et al.*, 1989, 1991). This inverse dependence of cosmic ray flux (and thus the nuclide production rate) on depth enables the erosion rate to be calculated from ^{10}Be and ^{26}Al abundances assuming a steady state between nuclide production, decay, and erosion:

$$E = \frac{\Lambda}{\rho}\left(\frac{P(h,\theta)}{C} - \lambda\right) \tag{8}$$

where E is the bedrock lowering rate (cm a^{-1}), Λ is the mean attenuation length of the target material (*c.* 165 g cm^{-2}), P is nuclide production rate at slope θ and beneath any soil depth h (atom a^{-1}), C is nuclide concentration (atom g^{-1}), and λ is the nuclide decay constant. Recent work shows that catchment-averaged erosion rates can be determined from cosmogenic nuclide abundances in alluvial sediments (Bierman and Steig, 1996; Granger *et al.*, 1996). In addition to soil production rates (equivalent to landscape lowering) across the field area, Heimsath *et al.* (1997) sampled stream sands and gravels in the channel immediately upstream of Haypress pond (identified as *creek2* in their table 1) for ^{10}Be and ^{26}Al, yielding a long-term basin-wide erosion rate of 102 ± 25 m Ma^{-1} for the basin studied here.

Results and Discussion

Pond sediment volume

Sediment thicknesses in Haypress Pond range from 0·85 m to 2·47 m, with the thickest deposits at the inlet of the Creek and generally thinning toward the dam (Figure 2). Observations of the sediment deposits subsequent to dam removal showed that the variation of sediment depths reflects a prograding delta beginning at the upstream end of the pond. We interpolated and integrated our sediment depth measurements, both from the points labelled and shown on Figure 2 and at points along the shoreline, to determine a total volume of 1060 m^3 of wet sediment. With annual precipitation of 760 mm, a catchment area of 33 ha, and the time-averaged pond water volume of 1100 m^3, Heinemann's (1981) curve shows a trap efficiency (*TE*) of 17 per cent. Dividing the retained sediment by the *TE* suggests that 6240 m^3 of sediment have been transported to the pond over its 42 ± 8 year lifespan (Table I). Using a measured dry bulk density (ρ_{br}) for the sediments of 700 kg m^{-3} in Equation 1 results in a total mass of $4{\cdot}4 \times 10^6$ kg for the eroded sediments. This mass loss is equivalent to a 40-year soil loss rate of $3{\cdot}2 \pm 0{\cdot}9$ t ha^{-1} a^{-1} for the catchment. Using Equation 2 with an average bulk density of 2200 kg m^{-3} for the weathered bedrock (Heimsath *et al.*, 1999), we converted this soil loss rate to an equivalent bedrock lowering rate of 143 ± 41 m Ma^{-1} (using the Bubnoff unit, equivalent to mm ka^{-1}, to keep units standard). While this catchment-averaged rate is higher than the long-term average rate of 102 ± 25 m Ma^{-1} determined for the same catchment by cosmogenic nuclide analyses (discussed below), it is in surprising agreement within the uncertainty of the measurements and the difference in temporal scale between the methods.

The relatively low *TE* determined for Haypress Pond reflects large annual inflow to pond-capacity ratio. This ratio does not take into account the flashy nature of the Haypress basin, where winter rainstorms (especially during El Nino years) coming off the Pacific can drop 200 mm of rain in a single week (Godt, 1999). The potentially high flow events for Haypress creek generated by such storms could mobilize stored pond sediment as well as enable suspended sediments to flow through the pond without settling. Given the absence of gauge data for Haypress creek, the Heinemann (1981) curve estimate of *TE* is based on annual precipitation and catchment area and is likely to be an overestimate of the pond's ability to hold sediment, as the Heinemann curve does not completely characterize the

DOI: 10.1002/esp

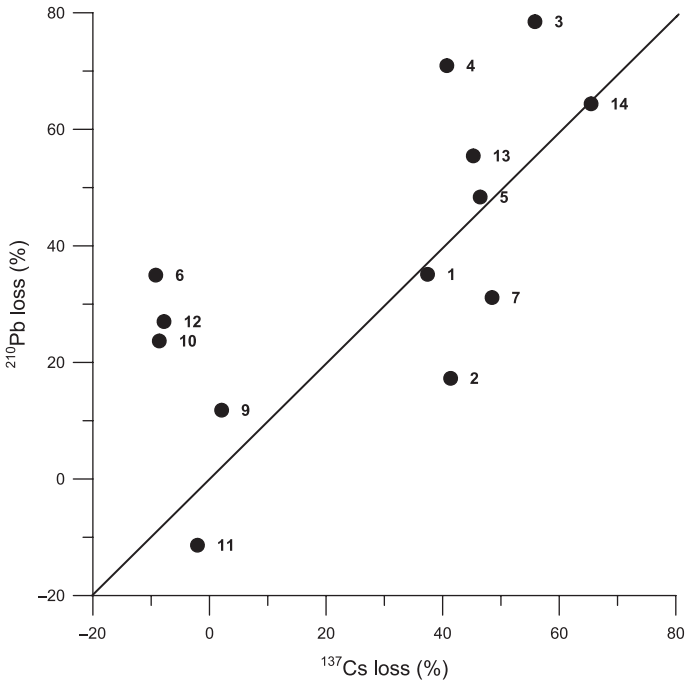

Figure 3. Plot of percentage ^{210}Pb reduction versus ^{137}Cs reduction for hillslope soil pits at the Haypress catchment. Pit numbers are posted adjacent to their respective point shown by black circle. Percentage reduction is relative to the stable sites at pits 9 and 11.

intra-annual variability in runoff. The erosion rate returned by pond sediment volume therefore has the potential to be an underestimate of the short-term erosion rates.

Fallout nuclides and soil loss

Fallout nuclide inventories for the 13 soil sampling pits, including the reference sites (pits 11 and 9), assumed to be experiencing relatively erosion, are reported in Table II. Mean percentage inventory reductions relative to the reference for ^{137}Cs and ^{210}Pb were 27 per cent and 37 per cent, respectively. There is clear agreement between the percentage reduction determined by ^{137}Cs and ^{210}Pb for each pit (Figure 3), supporting the assumption that the sediment transport processes are being similarly reflected by the nuclide inventories. Furthermore, since Pb is very insoluble, this result suggests that both Pb and Cs are mobilized by particle transport and, specifically, that ^{137}Cs is not geochemically mobile. Point rates of soil loss or gain returned by Equations 3 and 4 range from $-0{\cdot}7$ t ha^{-1} a^{-1} (pit 7) to $4{\cdot}8$ t ha^{-1} a^{-1} (pit 14) determined by the ^{137}Cs inventories, and $1{\cdot}3$ t ha^{-1} a^{-1} (pit 2) to $5{\cdot}7$ t ha^{-1} a^{-1} (pit 3), determined by the ^{210}Pb inventories. The average rates of soil loss for all the pits are $2{\cdot}0 \pm 0{\cdot}6$ t ha^{-1} a^{-1} (91 ± 30 m Ma^{-1} of bedrock loss) and $2{\cdot}7 \pm 0{\cdot}7$ t ha^{-1} a^{-1} (125 ± 33 m Ma^{-1}) derived from ^{137}Cs and ^{210}Pb, respectively.

When combined with these point rates, the topographic position of sampling sites (Figure 1) indicates the large degree of variability in erosion rate, even at small spatial scales. For example, pits 7 and 10 are *c*. 100 m apart but exhibit large variation that we attribute to differing dominant erosional processes. Pit 10 is located just off the ridge axis on a broad convex upland, while pit 7 is located just above a first-order channel, in an incipient hollow. This difference in landscape position subjects these two sites to very different sediment transport regimes, with pit 10 likely to be dominated by creep-like processes and pit 7 likely to be dominated by advective processes. As qualitative confirmation of this topographically based suggestion, observations two years after the initial study pits were excavated revealed that pit 7 had been filled with soil to within 5 cm of the land surface, while pit 10 was largely unchanged. These observations suggest that the excavation of pit 7 acted as a local sink for sediment being transported rapidly from upslope, either by overland flow processes, or by the random intersection of gopher burrows with the pit. We acknowledge that there is some heterogeneity in the deposition of radioactive fallout from the atmosphere that might effect our interpretations relating nuclide inventories to soil loss and physical processes. However, nuclide inventories at 14 points across contrasting topographical regimes in our basin ranged by a factor of >3, greatly

DOI: 10.1002/esp

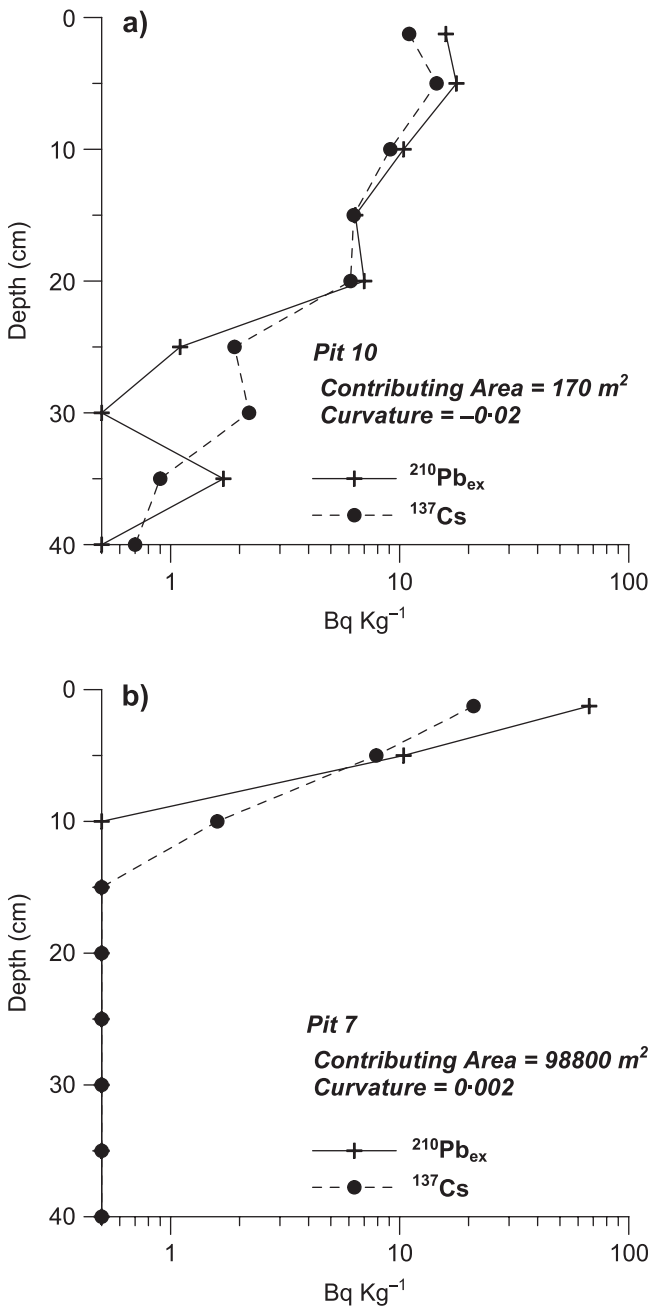

Figure 4. Detailed depth profiles of $^{210}Pb_{ex}$ and ^{137}Cs measured in samples from pit 10 (a) and pit 7 (b). Upslope contributing area and curvature are noted for each pit. Pit 10, and other profiles sampled on convex landforms, shows mixing of both short-lived nuclides to significantly deeper depths than pit 7, and other profiles sampled from convergent regions. These nuclide profiles quantify much stronger evidence for the diffusion-like mixing processes across the divergent regions versus the potential for overland flow processes in the convergent regions, which is consistent with field observations detailed in the text.

exceeding the 20 to 30% variability in inventory that has been attributed to depositional processes (Kaste *et al*., 2006; Sutherland *et al*., 1996).

We test the potential signatures of different transport processes on the nuclide activity profiles by examining depth profiles of nuclide inventory in detail (Kaste *et al*., 2006). Comparison of the activity depth profiles collected from pit 10 and pit 7 shows, for example, dramatically different nuclide signatures (Figure 4). In pit 10, an example of a

DOI: 10.1002/esp

pit where linear slope-dependent processes are likely to be dominant due to bioturbation as the dominant mixing and sediment transport process, both ^{137}Cs and ^{210}Pb inventories extend to depths of 40 cm. Conversely, at pit 7, an example of a pit where overland flow processes are likely to be dominant, there is no nuclide signal deeper than 10 cm. Both profiles exemplify the signature of different sediment transport processes observable with nuclide profiles, and are consistent with those reported for a rolling grassland landscape in Kansas (Kaste *et al*., 2006), as well as for a southeastern Australian landscape (Heimsath *et al*., 2002; Kaste *et al*., unpublished). Across those soil-mantled landscapes, the divergent ridges are dominated by bioturbation processes that fully mix the soil profile, while the convergent swales can be dominated by overland flow processes.

Fallout radionuclides yield point erosion rates for the upland part of the landscape. Since basin-wide rates calculated from our fallout radionuclide analyses are equivalent to rates determined from the pond sediment-derived rate, upland sediment storage is probably insignificant here. Furthermore, our measured fallout isotope inventories are consistent with or below inventories predicted from depositional models (Simon *et al*., 2004; Preiss *et al*., 1996). These observations suggest that soil is either stable or eroding, but not significantly aggrading in the uplands. We also note that these results strongly differ from agricultural landscapes, which often have substantial accumulation of sediment in concave areas that accumulate over relatively short timescales (Lowrance *et al*., 1988; Walling *et al*., 1999). Other workers do not observe morphometric evidence of potential storage reservoirs across the upland landscape of this sub-basin (Dietrich *et al*., 1995; Heimsath 1997, 1999). We believe it is reasonable, therefore, to assume complete sediment delivery to the pond.

Our sampling layout does not create a sufficiently dense grid to allow for calculation of a basin-wide rate through simple averaging of point rates. While scattered, our point soil loss rates do allow us to make inferences about dominant processes by examining the factors driving spatial variability in erosion rates.

Sediment transport processes from point rates and morphometry

Our radionuclide data support distinguishing between convex and concave regions of the landscape from a process perspective, as suggested by the motivation for Equations 5–7. Specifically, comparison of convex and concave percentage radionuclide depletion (combined ^{137}Cs and ^{210}Pb) using a one-way ANOVA indicates that these populations are significantly different within a 99 per cent confidence interval. Convex areas have a mean depletion of 33 per cent, while concave areas have a mean depletion of 65 per cent. This dramatic difference is despite convex areas being, on average, about 10° steeper than concave areas. By separating data from pits in the concave-up swales from the pits on the convex-up ridges, four trends can be used to test the conceptual framework outlined above for how the dominant sediment transport process depends on topographic position.

1. At convex sites, the average of erosion rates from ^{137}Cs and ^{210}Pb percentage inventory loss shows a positive linear correlation with local land-surface curvature (Figure 5a). The correlations for both ^{137}Cs and ^{210}Pb are significant at the 95 per cent confidence interval and support the dominance of slope-driven transport at convex sites, as predicted by Equation 5 and also shown by Heimsath *et al*. (1997, 1999) for the same field area using cosmogenic nuclide (^{10}Be and ^{26}Al) derived soil production rates and detailed measurements for topographic curvature. Figure 5a also supports the conclusion of Heimsath *et al*. (1997) that the landscape is not in a state of long-term dynamic equilibrium as even the short-term erosion rates increases with increasing convexity, suggesting that the ridge crests are flattening relative to the less convex side slopes.
2. Average of erosion rates from ^{137}Cs and ^{210}Pb percentage inventory loss shows a very weak positive power-law correlation with the left-hand side of Equation 7 (Figure 5b). The values of m and n that 'best' fit the data are 1 and 1·8, respectively, and were determined by plotting all the data for Figure 5b using the full range of exponents summarized in Prosser and Rustomji (2000) and determining which combination led to the best linear fit to the data. These exponents are consistent with erosion caused by unchannelled overland flow (Kirkby, 1969) and with field observations during winter storms (Dietrich *et al*., 1993; Prosser and Dietrich, 1995). This poor correlation may be due to the small range of drainage areas examined, from 0 ha to 0·33 ha. Because of this relative lack of correlation, and the sparseness of our sampling density, we use the mean value of 158 ± 32 m Ma^{-1} for erosion in concave areas when extrapolating to the Haypress Basin, as discussed below.
3. Using an independently derived value of 50 cm^2 a^{-1} (calculated for this site by Reneau, 1988; reported in McKean *et al*., 1993) for the proportionality constant used in the linear sediment transport law (K_d in Equations 5 and 6, commonly called the linear 'diffusivity') as applicable to the field area, and topographic curvatures from our 10 m DEM, we used Equation 6 to predict erosion rates for our convex sampling sites. There is remarkable agreement between the erosion rate determined by nuclide activities from the convex-up sample sites and the erosion rate predicted by simply multiplying the above proportionality constant by the local curvature

DOI: 10.1002/esp

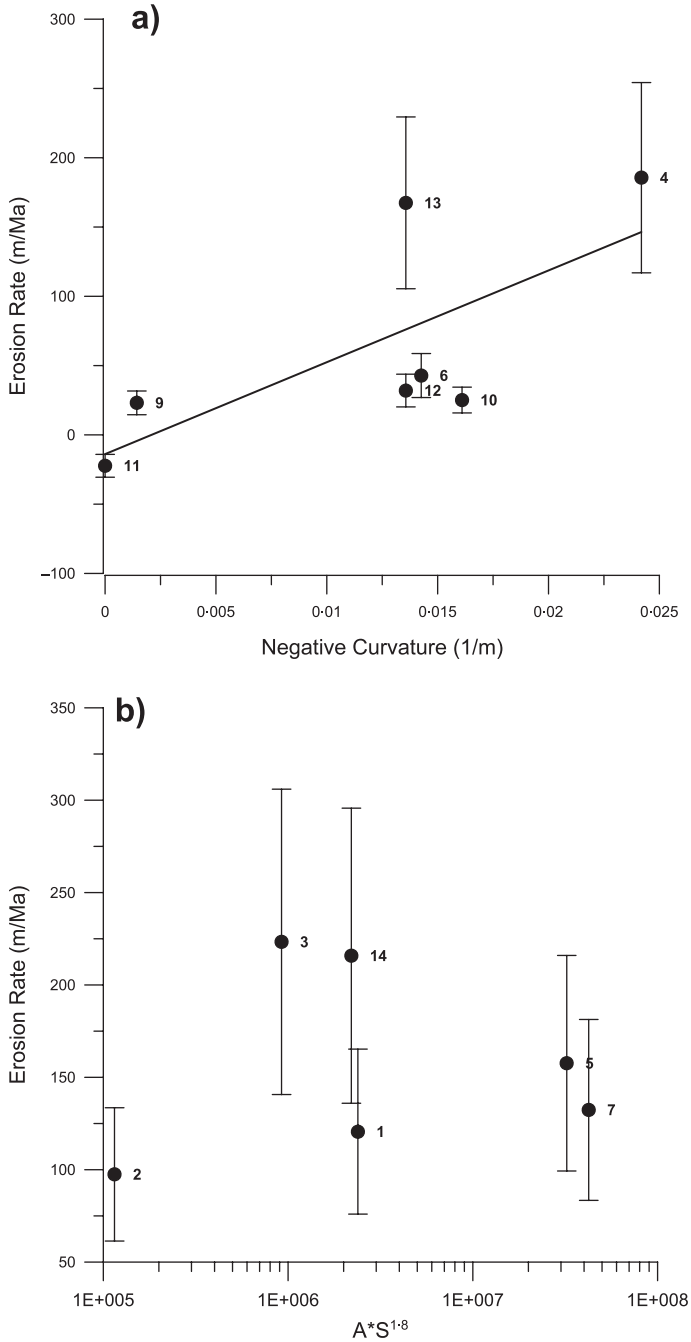

Figure 5. (a) Erosion rates determined from soil pits on convex-up topography versus negative local surface curvature (more strongly convex sites plot at higher values). Erosion rates are averages of rates determined by ^{137}Cs and ^{210}Pb activities using methodology described in the text. Pit numbers are posted adjacent to their respective point shown by black circle. Black line is the weighted best fit to the data used to extrapolate observed rates to all convex-up parts of the catchment. (b) Erosion rates from soil pits on concave-up topography versus the power-law product of contributing area and slope (Equation 7 in text, with m and n equal to 1 and 1·8, respectively). Erosion rates are averages of rates determined by ^{137}Cs and ^{210}Pb activities using methodology described in the text. Pit numbers are posted adjacent to their respective point shown with black circle. The poor correlation led to using the mean of 158 ± 32 m Ma^{-1} for all concave-up regions of the catchment.

DOI: 10.1002/esp

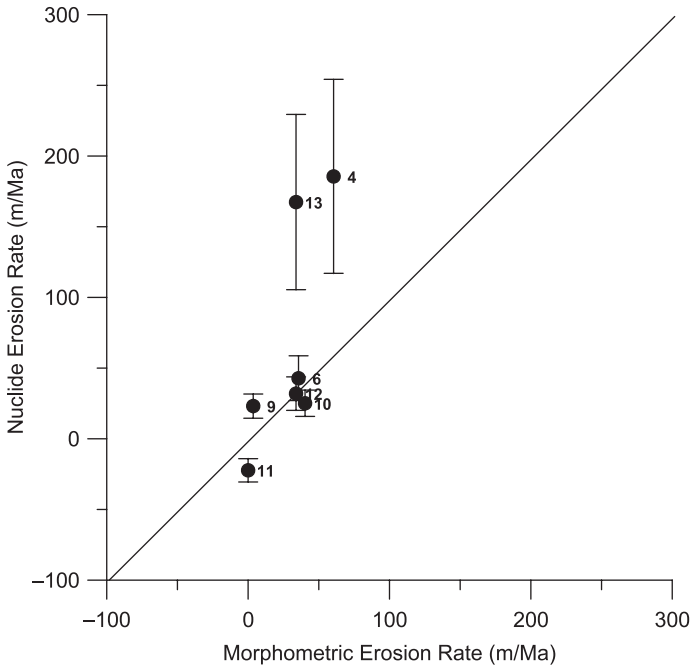

Figure 6. Plot of nuclide-based point erosion rates from soil pits on convex-up topography versus erosion rates predicted using a linear sediment transport law. Curvature-based erosion rate calculated using Equation 6 in the text, a linear slope-dependent 'diffusivity' of 50 $cm^2\ a^{-1}$ (Heimsath *et al.*, 1999), and local land surface curvature calculated using the high-resolution DEM for the catchment. The black line indicates 1:1 agreement and is not fitted to the data.

(Figure 6). That two such completely disparate methods show such clear agreement is an exciting endorsement for using the fallout-derived isotopes of ^{210}Pb and ^{137}Cs to quantify short-term erosion rates and sediment transport processes. It is interesting to note that the two pits (13 and 4) lying off the 1:1 line of Figure 6 are from the steeper regions of the catchment, as is pit 6. It is likely that the underestimate of the predicted rate using the linear transport function might be explained by the recent suggestion that an alternative transport relationship would be more appropriate (Heimsath *et al*., 2005).

4. We extrapolated nuclide inventories from the 13 point measurements to the entire landscape by using the relationship from Figure 5a for convex topography, where erosion rate is a function of local curvature and the average rate for the convex sampling sites was 79 ± 29 m Ma^{-1}. Concave cells were all assigned the average radionuclide erosion rate of 158 ± 32 m Ma^{-1} due to the lack of any discernible trend in Figure 5b. By extrapolating erosion rates from ^{137}Cs and ^{210}Pb for the Haypress basin based on this assignment of rates, we constructed a map of the spatial variability of these short-term rates (Figure 7). We also determined a basin-wide weighted average erosion rate of 136 ± 36 m Ma^{-1} by adding up the erosion rates determined by both ^{137}Cs and ^{210}Pb and assigned to every pixel used to generate Figure 7. We discuss the implications of the comparison of this rate to the rate determined from the pond sediment and cosmogenic nuclide data below. The difference in predicted erosion rate between concave (higher, nearly constant rate) and convex (lower, more variable rate) areas is the most striking feature of this map and is consistent with the modelling results of Dietrich *et al*. (1995) and the cosmogenic nuclide rates of Heimsath *et al*. (1997). From a process perspective this variability in erosion rates determined by short-lived nuclide analyses is consistent with vertical soil mixing observed at the convex sites, and overland flow processes dominating the convergent zones. Such differences in process mix fallout-derived nuclides into the soil column across the ridges, while preferentially removing the surface layers of sediment that have higher nuclide concentrations across the swales.

Cosmogenic nuclides

^{10}Be and ^{26}Al concentrations in Haypress Creek sediments (*creek2* in Heimsath *et al*., 1999) provide a long-term (*c*. 10 ka) estimate of basin-wide average erosion rate. Heimsath *et al*. (1999, table 1) present this basin-wide rate

DOI: 10.1002/esp

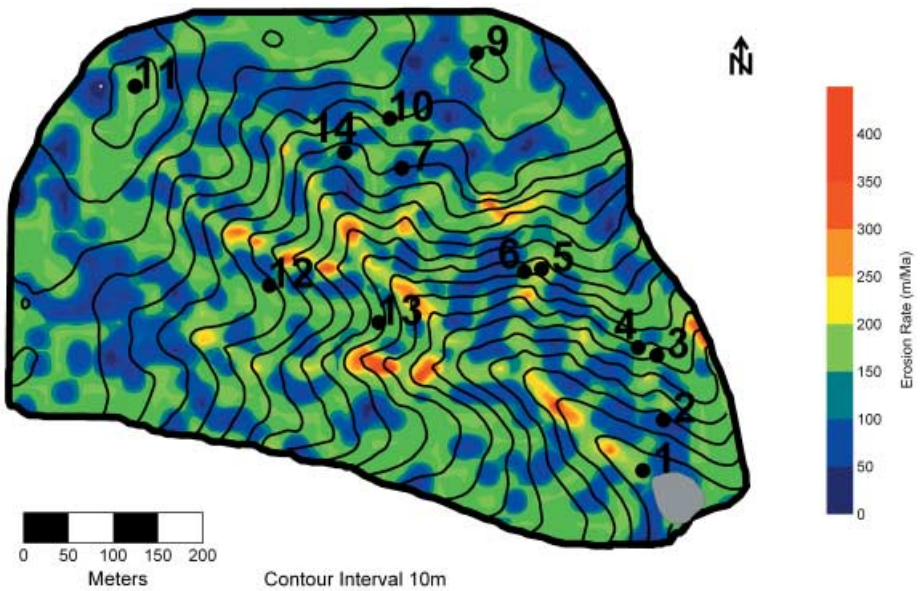

Figure 7. Map of extrapolated ^{137}Cs and ^{210}Pb erosion rates for the Haypress Basin. Soil pit locations are shown by black circles and labelled with pit numbers. Extrapolation from the point rates at the numbered soil pits to the entire basin is based on the correlation of erosion rate with curvature shown in Figure 5a for the pits on divergent topography, while a mean rate of 158 m Ma^{-1} was used for the pits on convergent topography. This figure is available in colour online at www.interscience.wiley.com/journal/espl

of 102 ± 25 m Ma^{-1} (2·3 ± 0·6 t ha^{-1} a^{-1}) as well as point erosion rates (i.e. soil production rates, which are equivalent to local land surface lowering rates) from hillslopes adjacent to the Haypress catchment. Point erosion rates from cosmogenic nuclides show a strong correlation between curvature and erosion rates, with negative curvature (divergent) areas showing the highest erosion rate. These results supported the use of the linear transport relationship (Equations 5 and 6) to model sediment transport processes on low gradient slopes. Our point erosion rates from fallout nuclides from the divergent ridges show a similar correlation, but also suggest that an alternate transport relationship may be more important for higher gradient slopes.

Implications

Process determination

The combination of ^{137}Cs and ^{210}Pb inventories with high-resolution digital elevation data opens up a new avenue in the use of fallout nuclides. Previous studies have used ^{7}Be ($t_{1/2} = 53{\cdot}3$ days) to infer the presence of sheetwash processes over very short timescales (Wallbrink and Murray, 1993; Walling *et al*., 1999) and have used DEM data to extrapolate ^{137}Cs inventories on the basis of slope (Walling *et al*., 2002). None have combined ^{137}Cs and ^{210}Pb correlations with landscape morphometry and geomorphic process laws to distinguish between different soil loss mechanisms. Fallout nuclides in erosion studies are already an excellent tool for identifying spatial variability in erosion rates at the basin scale (e.g. He and Walling, 1997; Porto *et al*., 2001). Our use of these nuclides to test how sediment transport processes can be quantified by different geomorphic transport relationships reveals exciting potential for further work that would expand upon the sampling scheme used here. Quantification of the dominant sediment transport processes would be especially useful for land managers. An understanding of the magnitude (from quantitative calibration relationships) and style (from correlation with local morphometry) of soil loss would, therefore, be an excellent tool in conserving the soil resource.

Specifically, we show here that sites dominated by overland flow processes experience higher rates of soil loss than those areas dominated by diffusion-like processes on short timescales. While some of this difference is attributable to the preferential removal of surface soil by the overland flow, and the resulting depletion of radionuclide activity, our observations of soil pit infilling two years after the initial study support the higher rates found at flow-dominated sites. This finding suggests that efforts to reduce hillslope erosion should focus on those areas subject to overland flow in

DOI: 10.1002/esp

Table III. Haypress catchment basin-wide erosion

Method	Erosion rate (m Ma^{-1})	±
Cosmogenic nuclides	102	25
Pond sediment	143	41
Spatially averaged ^{210}Pb	152	33
Spatially averaged ^{137}Cs	120	14

order to control soil loss most effectively. This suggestion also supports the land-management perspective that retarding slope-driven transport is likely to be difficult and costly, while changing runoff patterns might more easily reduce soil loss.

Comparisons of methods/timescales

To understand the long-term implications of the short-term rates and processes quantified here by using pond sediment volume and the fallout nuclides ^{137}Cs and ^{210}Pb, we compare these basin-wide rates with those determined using *in situ*-produced cosmogenic nuclides (Heimsath *et al*., 1997, 1999) (Table III). We interpret these results as showing broad agreement of erosion rates determined for both short and long timescales. The agreement between spatially averaged rates is strengthened by the fact that our use of ^{137}Cs and ^{210}Pb inventories showed correlation with landscape morphometry. Such morphometric correlation suggests that the short-term rates determined with fallout nuclides agree with the long-term processes shaping the landscape. Similarly, agreement between rates from pond sediment and fallout nuclides implies that over the last 40 years or so soil has been lost from the hillsides at the same rate that it has been delivered to Haypress pond. This conclusion is supported by previous modelling of soil depths in this area (Dietrich *et al*., 1995), and suggests that significant sediment storage is not occurring across the upland landscape. Specifically, this means that advective processes are removing sediment from the convergent regions as rapidly as the biogenic processes are producing and delivering sediment from the divergent ridges.

Studies in other areas have shown agreement (Gellis *et al*., 2004; Ferrier *et al*., 2005), underestimation (Meyer *et al*., 2001; Kirchner *et al*., 2001), and even overestimation (Hewawasam *et al*., 2003), when comparing short- with long-term rates. Relationships between observed decadal rates and rates inferred for the last 10 000 to 30 000 years are highly site-dependent. The agreement shown here between short- and long-term rates implies that forcing from climate (El Nino–Southern Oscillation), tectonics, and human impacts (100+ years of grazing) has either been insufficient to perturb the landscape or, in the case of tectonics, has a period of change too long to be resolved by our methods. Thus, the processes observed today in the coastal hills of Marin County are likely to be similar to those that have shaped the landscape for several thousand years, suggesting that infrequent, catastrophic events are off minor importance.

Acknowledgements

We thank Benjamin Burke and Jennifer Mygatt for field assistance, and the Golden Gate National Recreation Area for access to our study site. Two anonymous reviewers helped strengthen the paper considerably. We also thank Joanne Stewart, former rancher of Tennessee Valley, for information regarding historical land use patterns. This work was funded by the NSF EAR-0239655 and DEB-0128995, the Richter Memorial Trust, and the Dartmouth College Department of Earth Sciences.

References

Bierman PR. 1994. Using *in situ*-produced cosmogenic isotopes to estimate rates of landscape evolution; a review from the geomorphic perspective. *Journal of Geophysical Research B, Solid Earth and Planets* **99**(7): 13885–13896.

Bierman P, Steig EJ. 1996. Estimating rates of denudation using cosmogenic isotope abundances in sediment. *Earth Surface Processes and Landforms* **21**: 125–139.

Black TA, Montgomery DR. 1991. Sediment transport by burrowing animals, Marin County, California. *Earth Surface Processes and Landforms* **16**: 163–172.

Bonnet S, Crave A. 2003. Landscape response to climate change; insights from experimental modeling and implications for tectonic versus climatic uplift of topography. *Geology* **31**(2): 123–126.

Campbell D, Church M. 2003. Reconnaissance sediment budgets for Lynn Valley, British Columbia: Holocene and contemporary time scales. *Canadian Journal of Earth Sciences* **40**: 701–714.

Carson MA, Kirkby MJ. 1972. *Hillslope Form and Process*. Cambridge University Press, London.
Cerling TE, Craig H. 1994. Geomorphology and *in-situ* cosmogenic isotopes. *Annual Review of Earth and Planetary Sciences* **22**: 273–317.
Dietrich WE, Dunne T. 1978. Sediment budget for a small catchment in mountainous terrain. *Zeitschrift fur Geomorphologie* **29**: 191–206.
Dietrich WE, Wilson CJ, Montgomery DR, McKean J, Bauer R. 1992. Erosion thresholds and surface morphology. *Geology* **20**: 675–679.
Dietrich WE, Wilson CJ, Montgomery DR, McKean J. 1993. Analysis of erosion thresholds, channel networks, and landscape morphology using a digital terrain model. *Journal of Geology* **101**(2): 259–278.
Dietrich WE, Reiss R, Hsu M, Montgomery DR. 1995. A process-based model for colluvial soil depth and shallow landsliding using digital elevation data. *Hydrological Processes* **9**: 383–400.
Dietrich WE, Bellugi DG, Sklar LS, Stock JD, Heimsath AM, Roering JJ. 2003. *Prediction in Geomorphology*. Geophysical Monograph 135. AGU: 1–30.
Ferrier KL, Kirchner JW, Finkel RC. 2005. Erosion rates over millennial and decadal timescales at Caspar Creek and Redwood Creek, Northern California Coast Ranges. *Earth Surface Processes and Landforms* **30**: 1025–1038.
Flint LE, Curtis JA, Flint AL. 2003. Development of a hillslope-erosion-potential index for sediment transport in the Yuba River basin. *Abstracts with Programs – Geological Society of America* **35**(6): 433.
Fornes WL, Whiting PJ, Wilson CG, Matisoff G. 2005. Caesium-137-derived erosion rates in an agricultural setting: the effects of model assumptions and management practices. *Earth Surface Processes and Landforms* **30**: 1181–1189.
Gabet EJ. 2000. Gophur bioturbation: field evidence for non-linear hillslope diffusion. *Earth Surface Processes and Landforms* **25**(13): 1419–1428.
Gellis AC, Pavich MJ, Bierman PR, Clapp ER, Ellevein A, Aby S. 2004. Modern sediment yield compared to geologic rates of sediment production in a semi-arid basin, New Mexico: assessing human impact. *Earth Surface Processes and Landforms* **29**: 1359–1372.
Godt JW. 1999. *Maps showing locations of damaging landslides caused by El Nino rainstorms, winter season 1997–98, San Francisco Bay region, California*. United States Geological Survey Publication.
Granger DE, Kirchner JW, Finkel R. 1996. Spatially averaged long-term erosion rates measured from *in situ*-produced cosmogenic nuclides in alluvial sediment. *Journal of Geology* **104**(3): 249–257.
He Q, Walling DE, 1996. Interpreting the particle size effect in the adsorption of ^{137}Cs and unsupported ^{210}Pb by mineral soils and sediments. *Journal of Environmental Radioactivity* **30**: 117–137.
He Q, Walling DE. 1997. The distribution of fallout ^{137}Cs and ^{210}Pb in undisturbed and cultivated soils. *Applied Radioactive Isotopes* **48**(5): 677–690.
Heimsath AM, Dietrich WE, Nishiizumi K, Finkel RC. 1997. The soil production function and landscape equilibrium. *Nature* **388**: 358–361.
Heimsath AM, Dietrich WE, Nishiizumi K, Finkel RC. 1999. Cosmogenic nuclides, topography, and the spatial variation of soil depth. *Geomorphology* **27**: 151–172.
Heimsath AM, Chappell J, Spooner NA, Questiaux DG. 2002. Creeping soil. *Geology* **30**(2): 111–114.
Heimsath AM, Furbish DJ, Dietrich WE. 2005. The illusion of diffusion: Field evidence for depth dependent sediment transport. *Geology* **33**(12): 949–952.
Heinemann HG. 1981. A new sediment trap efficiency curve for small reservoirs. *Water Resources Bulletin* **17**(5): 825–830.
Hewawasam T, von Blanckenburg F, Schaller M, Kubik P. 2003. Increase of human over natural erosion rates in tropical highlands constrained by cosmogenic nuclides. *Geology* **31**(7): 597–600.
Huang CC, O'Connell M. 2000. Recent land-use and soil-erosion history within a small catchment in Connemara, western Ireland: evidence from lake sediments and documentary sources. *Catena* **41**: 293–335.
Kaste JM, Heimsath AM, Hohmann M. 2006. Quantifying sediment transport across and undisturbed prairie landscape using Caesium-137 and high-resolution topography. *Geomorphology.* DOI: 10.1016/J.GEOMORPH.2005.12.007.
Kirchner JW, Finkel RC, Riebe CS, Granger DE, Clayton JL, King JG, Megahan WF. 2001. Mountain erosion over 10 yr, 10 k.y., and 10 m.y. time scales. *Geology* **29**(7): 591–594.
Kirkby MJ. 1969. Erosion by water on hillslopes. In *Water, Earth and Man.* Chorley RJ (ed.). Methuen: London.
Lal D. 1991. Cosmic ray labeling of erosion surfaces: *in situ* nuclide production rates and erosion models. *Earth and Planetary Science Letters* **104**: 424–439.
Lavé J, Burbank D. 2004. Denudation processes and rates in the Transverse Ranges, southern California: Erosional response of a transitional landscape to external and anthropogenic forcing. *Journal of Geophysical Research – Earth Surface* **109**: F01006. DOI: 10.1029/2003JF000023.
Litvin LF, Zorina YF, Sidorchuk AY, Chernov AV, Golosov VN. 2003. Erosion and sedimentation on the Russian Plain; Part 1, Contemporary processes. *Hydrological Processes* **17**(16): 3335–3346.
Lowrance R, McIntyre S, Lance C. 1988. Erosion and deposition in a field forest system estimated using cesium-137 activity. *Journal of Soil and Water Conservation* **43**(2): 195–199.
Matisoff G, Bonniwell EC, Whiting PJ. 2002. Soil erosion and sediment sources in an Ohio catchment using beryllium-7, cesium-137, and lead-210. *Journal of Environmental Quality* **31**(1): 54–61.
McKean JA, Dietrich WE, Finkel RC, Southon JR, Caffee MW. 1993. Quantification of soil production and downslope creep rates from cosmogenic ^{10}Be accumulations on a hillslope profile. *Geology* **21**(4): 343–346.
McManus J, Duck RW. 1985. Sediment yield estimated from reservoir siltation in Ochil Hills, Scotland. *Earth Surface Processes and Landforms* **10**: 193–200.
Meyer GA, Pierce JL, Wood SH, Jull AJT. 2001. Fire, storms, and erosional events in the ldaho batholith. *Hydrological Processes* **15**(15): 3025–3038.

Montgomery DR, Dietrich WE. 1988. Where do channels begin? *Nature* **336**: 232–234.
Montgomery DR, Dietrich WE. 1989. Source areas, drainage density, and channel initiation. *Water Resources Research* **25**(8): 1907–1918.
Montgomery DR, Dietrich WE. 1994. A physically based model for the topographic control on shallow landsliding. *Water Resources Research* **75**(16): 1153–1171.
Neil DT, Mazari RK. 1993. Sediment yield mapping using small dam sedimentation surveys, southern Tablelands, New South Wales. *Catena* **20**: 13–25.
Nishiizumi K, Kohl CP, Arnold JR, Klein J, Fink D, Middleton R. 1991. Cosmic ray produced ^{10}Be and ^{26}A1 in Antarctic rocks: exposure and erosion history. *Earth and Planetary Science Letters* **104**: 440–454.
Nishiizumi K, Winterer EL, Kohl CP, Klein J, Middleton R, Lal D, Arnold JR. 1989. Cosmic ray production rates of ^{10}Be and ^{26}A1 in quartz from glacially polished rocks. *Journal of Geophysical Research B, Solid Earth and Planets* **94**(12): 17907–17915.
Nishiizumi K, Kohl CP, Arnold JR, Dorn R, Klein J, Fink D, Middleton R, Lal D. 1993. Role of *in situ* cosmogenic nuclides ^{10}Be and ^{26}A1 in the study of diverse geomorphic processes. *Earth Surface Processes and Landforms* **18**: 407–425.
Porto P, Walling DE, Ferro V. 2001. Validating the use of Caesium-137 measurements to estimate soil erosion rates in a small drainage basin in Calabria, Southern Italy. *Journal of Hydrology* **248**: 93–108.
Preiss N, Melieres MA, Pourchet M. 1996. A compilation of data on lead 210 concentration in surface air and fluxes at the air-surface and water-sediment interfaces. *Journal of Geophysical Research-Atmospheres* **101**(D22): 28847–28862.
Prosser IP, Rustomji P. 2000. Sediment transport capacity relations for overland flow. *Progress in Physical Geography* **24**: 179–193.
Prosser IP, Dietrich WE, Stevenson J. 1995. Flow resistance and sediment transport by concentrated overland-flow in a grassland valley. *Geomorphology* **13**(1–4): 71–86.
Prosser IP, Dietrich WE. 1995. Field experiments on erosion by overland flow and their implication for a digital terrain model for channel initiation. *Water Resources Research* **31**(11): 2867–2876.
Rantz SE. 1968. *Average annual precipitation and runoff in north coastal California*. United States Geological Survey Hydrological Atlas 298, scale 1:1,000,000.
Reneau SL. 1988. *Depositional and erosional history of hollows: application to landslide location and frequency, long-term erosion rates, and the effects of climatic change*. PhD Thesis, University of California, Berkeley.
Reneau SL, Dietrich WE, Wilson CJ, Rogers J. 1984. Colluvial deposits and associated landslides in the northern San Francisco Bay area, California, USA. *IV International Symposium on Landslides*, Downsview, ON, Canada: 425–430.
Reneau SL, Dietrich WE, Donahue DJ, Jull AJT, Rubin M, 1990. Late Quaternary history of colluvial deposition and erosion in hollows, Central California Coast Ranges. *GSA Bulletin* **102**(7): 969–982.
Roering JJ, Almond P, Tomkin P, McKean J. 2002. Soil transport driven by biological processes over millenial time scales. *Geology* **30**: 1115–1118.
Simon SL, Bouville A, Beck HL. 2004. The geographic distribution of radionuclide deposition across the continental US from atmospheric nuclear testing. *Journal of Environmental Radioactivity* **74**(1–3): 91–105.
Sutherland RA. 1996. Caesium-137 soil sampling and inventory variability in reference locations: A literature survey. *Hydrological Processes* **10**(1): 43–53.
Van den Wall Bake GW. 1986. Siltation and soil erosion survey in Zimbabwe. In *Drainage Basin Sediment Delivery* (Proceedings of the Albuquerque Symposium, August 1986). Publication No. 159. IAHS: 69–80.
Verstraeten G, Poesen J. 2000. Estimating trap efficiency of small reservoirs and ponds: methods and implications for the assessment of sediment yield. *Progress in Physical Geography* **24**(2): 219–251.
Verstraeten G, Poesen J. 2002. Using sediment deposits in small ponds to quantify sediment yield from small catchments: possibilities and limitations. *Earth Surface Processes and Landforms* **27**: 1425–1439.
Wahrhaftig C. 1984. Structure of the Marin Headlands block, California: a progress report. *Franciscan Geology of Northern California* **43**: 31–50.
Wallbrink PJ, Murray AS. 1993. Use of fallout radionuclides as indicators of erosion processes. *Hydrological Processes* **7**: 297–304.
Wallbrink PJ, Murray AS. 1996. Determining soil loss using the inventory of excess Lead-210 to Cesium-137. *Soil Science Society of America Journal* **60**: 1201–1208.
Walling DE, He Q. 1999. Improved models for estimating soil erosion rates from cesium-137 measurements. *Journal of Environmental Quality* **28**: 611–622.
Walling DE, He Q, Blake W. 1999. Use of Be-7 and Cs-137 measurements to document short- and medium-term rates of water-induced soil erosion on agricultural land. *Water Resources Research* **35**(12): 3865–3874.
Walling DE, Russell MA, Hodgkinson RA, Zhang Y. 2002. Establishing sediment budgets for two small lowland agricultural catchments in the UK. *Catena* **47**: 323–353.
Walling DE, Collins AL, Sichingabula HM. 2003. Using unsupported Lead-210 measurements to investigate soil erosion and sediment delivery in a small Zambian catchment. *Geomorphology* **52**: 193–213.
Whipple KX, Tucker GE. 1999. Dynamics of the stream-power river incision model: Implications for the height limits of mountain ranges, landscape response timescales, and research needs. *Journal of Geophysical Research* **104**(B8): 17661–17674.
Wilson CJ, Dietrich WE. 1987. The contribution of bedrock groundwater flow to storm runoff and high pore pressure development in hollows. *Erosion and Sedimentation in the Pacific Rim.* Publication No. 165. IAHS.
Zhang X, Walling DE, Quine TA, Wen A. 1997. Use of reservoir deposits and caesium-137 measurements to investigate the erosional response of a small drainage basin in the rolling Loess Plateau region of China. *Land Degradation and Development* **8**(1): 1–16.

DOI: 10.1002/esp